JOURNAL OF CHEMICAL INFORMATION AND MODELING

Article

pubs.acs.org/jcim

AlphaSpace: Fragment-Centric Topographical Mapping To Target Protein−Protein Interaction Interfaces

David Rooklin,[†] Cheng Wang,[†] Joseph Katigbak,[†] Paramjit S. Arora,[†] and Yingkai Zhang*[,†,‡]

[†]Department of Chemistry, New York University, New York, New York 10003, United States

[‡]NYU-ECNU Center for Computational Chemistry at NYU Shanghai, Shanghai 200062, China

Supporting Information

ABSTRACT: Inhibition of protein−protein interactions (PPIs) is emerging as a promising therapeutic strategy despite the difficulty in targeting such interfaces with drug-like small molecules. PPIs generally feature large and flat binding surfaces as compared to typical drug targets. These features pose a challenge for structural characterization of the surface using geometry-based pocket-detection methods. An attractive mapping strategy—that builds on the principles of fragment-based drug discovery (FBDD)—is to detect the fragment-centric modularity at the protein surface and then characterize the large PPI interface as a set of localized, fragment-targetable interaction regions. Here, we introduce AlphaSpace, a computational analysis tool designed for fragment-centric topographical mapping (FCTM) of PPI interfaces. Our approach uses the alpha sphere construct, a geometric feature of a protein's Voronoi diagram, to map out concave interaction space at the protein surface. We introduce two new features—alpha-atom and alpha-space—and the concept of the alpha-atom/alpha-space pair to rank pockets for fragment-targetability and to facilitate the evaluation of pocket/fragment complementarity. The resulting high-resolution interfacial map of targetable pocket space can be used to guide the rational design and optimization of small molecule or biomimetic PPI inhibitors.

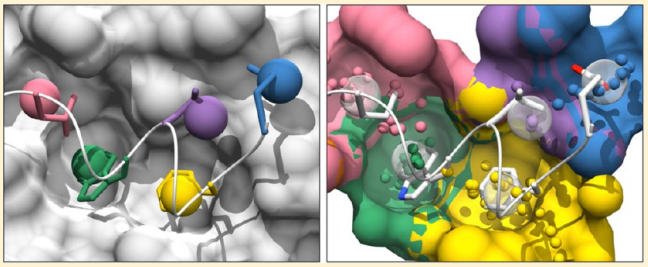

INTRODUCTION

Various protein−protein interaction inhibitors (iPPIs) are in development to treat cancer,[1−3] neurodegenerative disease,[4,5] autoimmune disease,[6,7] arthritis,[8] viral infection,[9,10] bacterial infection,[11] etc., and several have advanced into clinical trials and beyond.[2] Historically, PPI interfaces have been considered comparatively intractable drug targets for typical drug-like molecules.[12−14] But over the past decade, several approaches including screening of natural product-like compounds,[15,16] mimicry of protein interfaces,[17,18] and fragment-based drug discovery (FBDD)[19,20] have offered tangible success. FBDD allows for the identification of small weakly binding chemical fragments, which can be subsequently linked or extended into unique multi-fragment scaffolds.[21,22] Fragment-based approaches have led to the discovery of several high-affinity inhibitors[23] that are highly complementary to the distinct PPI interfaces they target,[23−25] and the tightest binders attain picomolar affinities.[26,27]

Alanine scanning mutagenesis[28,29] is commonly used to identify residues that interact most favorably in a PPI complex. These interactions, between individual hot spot residues and the partner protein, are reminiscent of a fragment-centric view of the PPI interface. Clusters of hot spot residues can serve as promising starting points for the design of small molecule iPPIs,[30] and biomimetic iPPIs are often designed specifically to preserve these hot spot interactions and to optimize them.[31−33] While identification of the important side chains can provide a good starting point for PPI inhibitor design, alanine scanning does not provide structural information about the surface involved in a hot spot interaction or the degree of complementarity between the surface and the side chain binding fragment. Thus, from an inhibitor design perspective, whether using FBDD or the alanine scanning technique, it is of significant interest and importance to obtain fragment-centric structural mapping of the target interfaces.

Mapping of PPI interfaces is closely related to the problem of ligand binding site detection. Over the years, a number of diverse algorithms have been developed for this purpose, which fall into four general categories: geometry-based,[30−32] probe-based,[37−40] grid-based,[41−49] and docking-based.[50−53] Some methods rely on the structure alone, while others incorporate energetic terms or sequence conservation into the pocket detection. Examples from all categories perform strongly when detecting classical ligand binding pockets, which are often large isolated cavities in the protein surface with well-defined concavity.[50,54,55] Some of these methods have been applied to investigate PPI interfaces, such as Q-SiteFinder[25] (a grid-based pocket detection method), FTMap[56−59] (a docking-based solvent-mapping method), and FindBindSite[51] (a ligand/fragment-docking-based method), all of which reveal that PPI interfaces are not adequately described by a single cavity, but

Received: February 24, 2015
Published: July 30, 2015

DOI: 10.1021/acs.jcim.5b00103
J. Chem. Inf. Model. 2015, 55, 1585−1599

comprise multiple interaction regions. On the other hand, the grid- and structure-based method DoGSite[60,61] has applied the concept of subpockets to demonstrate that a higher-resolution characterization of classical ligand binding pockets is generally feasible and practical, however this approach has yet to be applied to PPI interfaces.

Because PPIs often feature large and flat binding surfaces, without the deep pockets of typical drug targets, they pose a distinct challenge for geometry-based pocket-detection methods in providing a meaningful fragment-centric structural characterization. For example, the application of three popular geometry-based methods (CASTp,[34] fpocket,[36] and single linkage clustering similar to SiteFinder[62]) to characterize two established druggable PPI interfaces—Mdm2/p53[63,64] and Bcl-xL/Bak[65,66]—results in inconsistent definitions of pocket profiles (see Figure S1). The results do not represent the fragment-centric interactions observable at the interfaces and suggest a limited utility of the methods from a FBDD perspective. We observe three specific limitations: incomplete interface coverage, pocket expansion into solvent-inaccessible regions, and overconsolidation of pocket space across multiple side chain interactions, which lowers the resolution of the interfacial characterization.

In order to address the above limitations, we have developed AlphaSpace, a new computational analysis tool that features a fast geometry-based approach to provide a comprehensive fragment-centric topographical mapping of the PPI interface. AlphaSpace follows in the footsteps of fpocket[36] and MOE's SiteFinder[62] by using alpha spheres, a geometric feature of a protein's Voronoi diagram, to map out concave interaction space at the surface of a protein. Prior to these, the application of Voronoi tessellation to cavity detection originated in the pioneering work of Liang et al. and was first implemented in the CAST program.[67] However, AlphaSpace is unique among these existing Voronoi-based methods in its general divergence from a cavity-centric paradigm toward a fragment-centric and full-surface paradigm. Central to our approach are two new features, alpha-atom and alpha-space, and the new concept of the alpha-atom/alpha-space pair, which we utilize to rank interaction regions for fragment-targetability and to evaluate pocket/fragment complementarity to guide fragment optimization. Additional AlphaSpace components, including *Pocket matching* and *Pocket communities*, extend the fragment-centric methodology to establish a flexible pocket model and to identify highly targetable protein surface regions.

In the following sections, first, we present the methodology behind AlphaSpace fragment-centric topographical mapping (FCTM) and highlight aspects that enable AlphaSpace to reveal the fragment-centric modularity at PPI interfaces and to quantitatively evaluate fragment-centric pockets. For the initial section of the Results, we apply FCTM to the well-studied Mdm2/p53 PPI interface, discussing the utility of fragment-centric inhibitor design features. FCTM results are compared with the corresponding interaction regions detected using fpocket and FTMap. In the second section of the Results, we evaluate the performance of AlphaSpace on a larger data set of 12 PPI, 12 iPPI, and 9 apo structures from the 2P2I database.[68,69] Finally, we discuss a more general perspective on the AlphaSpace methodology and present conclusions.

METHODS

The central geometric construct employed by AlphaSpace is alpha sphere, a geometric feature derived from the Voronoi diagram of a set of points in three-dimensional space.[70] The Voronoi diagram is a tessellation of the space containing the points into a set of Voronoi cells, or polyhedrons, formed from planes that bisect adjacent points from the set. The alpha sphere centers are defined at the vertices of this tessellation. Each alpha sphere center will be an intersection of six bisecting planes and equidistant to exactly four points from the set. The concept of applying Voronoi tessellation to protein structure was first introduced by Richards in 1974,[71] along with the "weighted" Voronoi tessellation, a variation in the calculation to account for different atomic radii that was later implemented by Liang et al. in CAST.[67] AlphaSpace employs the "classical" Voronoi tessellation, also used by fpocket,[36] for which all atoms are treated as equivalent points. In this case, the alpha sphere makes contact with the centers of exactly four atoms but is otherwise empty of other atomic centers. Its radius is measured from alpha sphere center to atom center. Alpha spheres centered outside the protein surface mark concave surface regions and can be used to represent potential interaction space. Figure 1A illustrates how a Voronoi diagram can be used to map the concave interaction space in a two-dimensional schematic model of shallow pockets in a surface.

With AlphaSpace, we introduce two additional alpha sphere-related geometric features: alpha-atom and alpha-space (Figure 1B,C). An alpha-atom shares a center with its associated alpha sphere but with a reduced radius set to 1.8 Å. An alpha-atom can be thought of as a theoretical ligand atom at a discrete

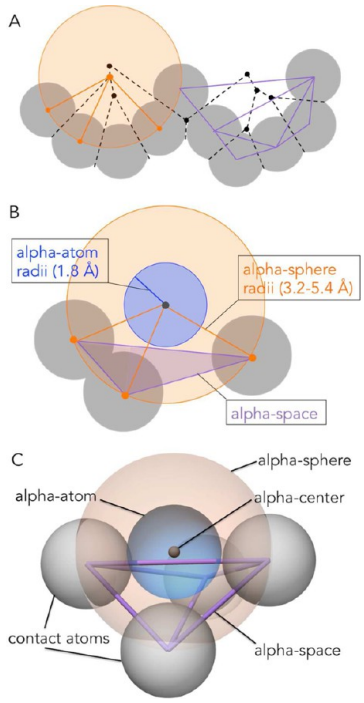

Figure 1. (A) Two-dimensional schematic of two fragment-centric pockets in a protein surface. Dashed black lines represent edges from the Voronoi tessellation. Black points are the Voronoi vertices, or alpha sphere centers. A single alpha-sphere is represented in orange. The Delaunay triangulation for one pocket is shown in purple; its total contiguous area (or volume, in 3-dimensions) is the total "alpha-space" for that pocket and is used to calculate pocket score. (B) An individual alpha-system: alpha sphere (orange), alpha-atom (blue), alpha-space (purple), and contact atoms (gray). (C) An individual alpha-system in three-dimensions, colored as in (B).

DOI: 10.1021/acs.jcim.5b00103
J. Chem. Inf. Model. 2015, 55, 1585−1599

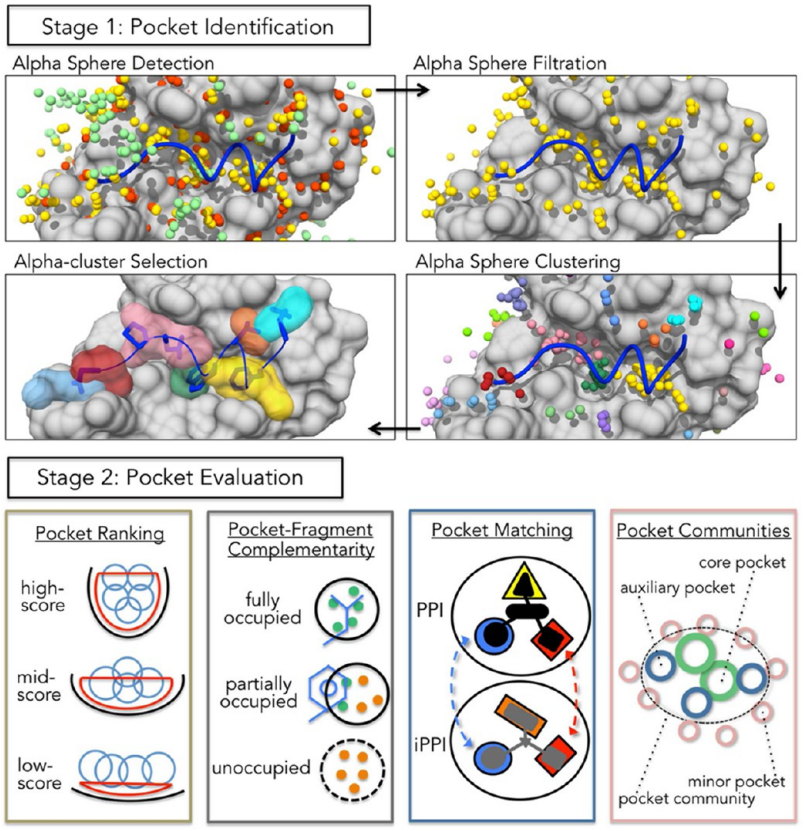

Figure 2. Overview for the two stages of fragment-centric topographical mapping (FCTM). Stage 1: Pocket Identification—*Alpha Sphere Detection*: all alpha sphere centers are shown and colored by radius (orange, r < 3.2 Å; yellow, 3.2 Å < r < 5.4 Å; green, r > 5.4 Å). *Alpha Sphere Filtration*: remove alpha spheres outside the minimum or maximum radius cutoffs. *Alpha Sphere Clustering*: alpha spheres are clustered into fragment-centric pockets (colored by alpha-cluster). *Alpha-cluster Selection*: only alpha-clusters in contact with the peptide or ligand are selected for evaluation (alternatively the selection can be expanded to include unoccupied pockets near the interface). Stage 2: Pocket Evaluation—includes *Pocket ranking* by AlphaSpace pocket score, *Pocket-fragment complementarity* to evaluate the percentage occupation of each pocket, *Pocket matching* between different structures of the protein, and *Pocket communities* to identify potentially druggable surface regions.

interaction point, positioned to make approximate contact with the small region of protein surface associated with the set of four alpha sphere contact atoms. The alpha-space is the volume of the tetrahedron defined by the centers of the four alpha sphere contact atoms. Every alpha-atom has an associated alpha-space, the volume of which captures information about the relative positions of the four contact atoms, which is related to the structure of the surface region associated with these four atoms. The set of all alpha-spaces for a set of points is equivalent to its Delaunay triangulation, the dual graph of the Voronoi diagram.

AlphaSpace fragment-centric topographical mapping (FCTM) is performed in two stages: pocket identification and pocket evaluation, as shown in Figure 2.

Stage 1: Pocket Identification. The first stage, pocket identification, consists of four consecutive steps:

I. *Alpha Sphere Detection.* All alpha spheres are identified from the Voronoi tessellation of a protein structure. This step is the same as fpocket[36] and MOE's Site Finder.[62] We employ the python wrapper to Qhull,[72] available in the SciPy package,[73] to calculate the Voronoi diagram.

II. *Alpha Sphere Filtration.* Identified alpha spheres are filtered by radius to remove from the analysis spheres deemed too small to represent solvent-accessible space (3.2 Å is set as the default minimum radius cutoff, Figure S2C) or too large to accurately represent space within contact proximity of the protein surface (5.4 Å is set as the default maximum radius cutoff, Figure S2B). These filtration parameters, which deviate from the corresponding default parameters in fpocket (3.0 and 6.0 Å, respectively), have been optimized to restrict our mapping to include only solvent-accessible space near the surface of the protein.

III. *Alpha Sphere Clustering.* Remaining alpha spheres are clustered into pockets, or "alpha-clusters", using an average linkage algorithm to restrict individual pocket size to represent small, fragment-centric interaction spaces.

IV. *Alpha-Cluster Selection.* Pockets at the PPI interface, or within an expanded interface, are then selected for subsequent quantitative evaluation.

In comparison with fpocket[36] and MOE's Site Finder,[62] the main deviation of AlphaSpace within this pocket identification stage is in the third step, alpha sphere clustering, where we employ an average linkage algorithm with an optimized clustering parameter to achieve a fragment-centric mapping. Because of the subtlety in fragment-centric structural modularity at PPIs, there is often not a well-defined gap within the flow of alpha spheres across the surface. This is why fpocket's multi-step clustering algorithm[36] (which includes a multiple linkage step set to 2 by default) and SiteFinder's single linkage clustering algorithm[62] are observed to extend individual

DOI: 10.1021/acs.jcim.5b00103
J. Chem. Inf. Model. 2015, 55, 1585−1599

pocket space across multiple fragment or side chain interactions (Figure S1). AlphaSpace, alternatively, clusters filtered alpha spheres into localized pockets, or alpha-clusters, using the average linkage routine in the SciPy hierarchical clustering package.[73] The algorithm uses the pairwise alpha sphere Euclidian distance matrix to generate a dendrogram according to the average-linkage criterion (Figure S3). The clustering parameter, which is the maximum mean distance between elements of any single cluster, determines where to cut this tree and, thus, the general size and final number of alpha-clusters in the topographical map. Here, by considering amino acid side chains to be the natural binding fragments in PPIs, we fit this clustering parameter to yield, on average, one alpha-cluster for every side chain engaged in a PPI. As shown in Figure S4, the average number of side chains per pocket is near unity when the maximum average linkage distance is within the range 4.6 to 4.8 Å. We set the default value of this parameter to be 4.7 Å.

Besides the third clustering step, the fourth step, alpha-cluster selection, also marks a conceptual break from the fpocket algorithm. Fpocket, as a more classical cavity-centric pocket detection method, aims to identify the most significant individual pockets as probable enzymatic active sites or ligand binding pockets. This leads to incomplete coverage for PPI interfaces, where many of the interactions involve smaller and shallower fragment-centric pockets. AlphaSpace, alternatively, does not screen pockets by number of alpha spheres but detects contact with the molecular binding partner to select for the array of alpha-clusters engaged in the PPI. This provides a landscape-like topographical map with extensive coverage of the interaction interface. Furthermore, in AlphaSpace, adjacent interaction regions are represented simultaneously as discrete alpha-clusters and as overlapping pockets, with shared pocket atoms along their boundaries. We leverage this pocket overlap to moderate the expansion of interface contact maps to reveal unoccupied targetable pockets near interaction interfaces.

Stage 2: Pocket Evaluation. Selected pockets from the first stage are quantitatively characterized in Stage 2 of AlphaSpace FCTM. The analysis includes *Pocket ranking*, *Pocket-fragment complementarity*, *Pocket matching*, and *Pocket communities*, as illustrated in Figure 2. Pocket evaluation is facilitated by the alpha-atom and alpha-space features and provides a high-resolution map of underutilized and targetable pocket space at a PPI interface.

We use alpha-space as a geometric feature related to the size and shape of a localized region of protein surface. The size of an individual alpha-space reflects the surface area and curvature of the small surface region associated with the set of four alpha sphere "contact" atoms (Figure 1). While the set of alpha spheres in an alpha-cluster will overlap, the corresponding set of alpha-spaces will fit face-to-face to form a contiguous volume. This allows for the sum over all alpha-spaces within a pocket to serve as a single metric that approximates the surface area and curvature of the complete pocket. Figure S5 illustrates the geometric relationship between the alpha-atom and the alpha-space in the context of an alpha-cluster (the Trp92 pocket from Mdm2/p53).

The alpha-atom construct can be used to calculate the alpha-cluster contact surface area (ACSA) for each individual pocket. When alpha spheres are clustered to define a pocket, the corresponding alpha-atoms form an overlapping alpha-cluster, the outline of which represents the approximate shape and size of that pocket's complementary pseudofragment (Figure 3). To calculate the atomistic ACSAs for an individual pocket, we use

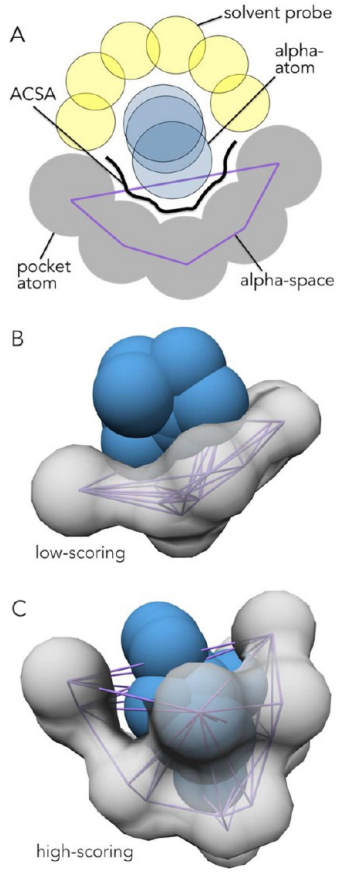

Figure 3. (A) Two-dimensional schematic depicting components used to calculate pocket score; solvent probes (yellow) and alpha-atoms (blue) are used to calculate the alpha-cluster contact surface area (ACSA) (black) of the pocket atoms (gray). The outline of the pocket alpha-space is purple. Below, alpha-atom and alpha-space representations for a low-scoring, shallow pocket (B) and for a high-scoring, deep pocket (C).

Naccess[74] to calculate the atomistic accessible surface areas for the protein structure alone and then for the same protein in complex with that pocket's single alpha-cluster. Subtracting the atomistic values associated with the alpha-cluster complex from the corresponding atomistic values associated with the protein alone will yield non-zero (and positive) values only for the set of atoms in direct contact with the alpha-cluster. These differences are taken as the atomistic surface areas associated with that individual pocket. The sum of these atomistic values provides the total ACSA for that pocket.

Pocket Ranking. Given a pocket J, we calculate its pocket score with the following formula:

$$\text{score}_J = \sum_{\alpha \in J} \left(V_\alpha \times \frac{\sum_{i \in \alpha} (\text{ACSA}_{i,J} \times \text{NP}_{i,J})}{\sum_{i \in \alpha} \text{ACSA}_{i,J}} \right)$$

where α is an alpha-space within pocket J with volume V_α, $\text{ACSA}_{i,J}$ is the alpha-cluster contact surface area for atom i calculated using alpha-cluster J (for each alpha-space we sum over the four corresponding alpha sphere contact atoms), and $\text{NP}_{i,J}$ is the binary polarity status for atom i in pocket J (1 for nonpolar atoms and 0 for polar atoms). Conceptually, the pocket score is equivalent to the pocket's nonpolar-weighted alpha-space volume. The score was developed as a single term to correlate well with a combination of nonpolar surface area

DOI: 10.1021/acs.jcim.5b00103
J. Chem. Inf. Model. 2015, 55, 1585−1599

and pocket curvature, two structural/chemical features previously shown to reflect a pocket's maximal binding potential.[75] Pocket score development details are described in the Supporting Information, Section S4, and Figures S12−14.

Pocket-Fragment Complementarity. If pocket J is engaged in a PPI or iPPI, we assess the structural complementarity between the pocket and the bound chemical fragment with the following formula:

$$\%\mathrm{occ}_J = \frac{\sum_{\alpha \in J} (V_\alpha \times O_\alpha)}{\sum_{\alpha \in J} V_\alpha}$$

where $\%\mathrm{occ}_J$ is the percentage of the interaction space of pocket J that is occupied by the bound ligand, α is an alpha-space within pocket J with volume V_α, and O_α is the binary occupation status of α (1 if occupied and 0 if unoccupied). Conceptually, we are partitioning the total alpha-space of the pocket into occupied space and unoccupied space by leveraging the discrete nature of each alpha-atom/alpha-space pair. Thus, the alpha-space occupation status is mediated through the position of its corresponding alpha-atom. Alpha-space occupation is conferred by spatial overlap between its alpha-atom and an atom from the bound ligand molecule, evaluated using a 1.6 Å cutoff distance measured between the centers of the alpha-atom and the ligand atoms. This cutoff is designed to be just longer than an average carbon−carbon bond length so that an unoccupied alpha-atom should represent a targetable interaction space, able to accommodate at least a methyl extension to the ligand, given the proper structure and chemistry of the evolving ligand.

Pocket Matching. In order to match similar fragment-centric pockets among different structures of the same protein, we calculate an $n \times n$ distance matrix, where n is the total number of interface pockets among all structures included in the matching. *Pocket matching* can be applied to any number of structures collectively. To calculate a pairwise pocket distance, $d_{J,K}$, between pockets J and K, we represent each pocket's ACSA as an array of length i, where i is the total number of heavy atoms found in the protein structure, containing the i atomistic ACSAs for each pocket—this vector will be non-zero only for the set of atoms in contact with that pocket's alpha-cluster. Our distance metric is inspired by the Jaccard distance, a statistic used for evaluating the dissimilarity between sample sets, and is implemented as

$$d_{J,K} = \frac{\sum_i |\mathrm{ACSA}_{i,J} - \mathrm{ACSA}_{i,K}|}{\sum_i \{\mathrm{ACSA}_{i,J} + \mathrm{ACSA}_{i,K}\}}$$

where the sum of all nonshared ACSA between pocket J and pocket K is divided by the total ACSA of pocket J and pocket K. This formula approximates the portion of the total pocket surface area that is dissimilar between the two pockets; values will range from 0, the distance between two identical pockets, to 1, the distance between two pockets with zero shared atoms. Additionally, for every pair of pockets from the same structure, the pocket distance is artificially set to a large value of 10, which is to avoid matching pockets within the same structure. From the calculated pairwise pocket distance matrix, the average linkage hierarchical clustering approach is employed to decompose all pockets into clusters, for which the distance clustering parameter is set to 0.75 by default. All pockets within one cluster are considered to be matched, and the pairwise pocket similarity, $s_{J,K}$, is evaluated as $1 - d_{J,K}$.

This *Pocket matching* approach serves as the foundation for an alignment-free flexible pocket model, a concept previously explored by Eyrisch and Helms to track pockets across a molecular dynamics trajectory.[76] A pocket cluster defines a flexible pocket entity, in which the mutual similarity describes an intrinsic degree of structural integrity, while differences among individual pockets within the cluster indicate structural flexibility.

Pocket Communities. Druggable PPI interfaces are typically defined by multiple fragment targetable interaction regions in close proximity, which often include one or several particularly important anchor interactions.[57,77−79] Inspired by this anchor/satellite interaction concept, we have developed a *Pocket community* feature to detect potentially druggable protein surface regions. First, all quantified pockets are classified as core, auxiliary, or minor pockets by employing AlphaSpace pocket score, for which the core and auxiliary pocket score cutoffs are set to 100 and 30 by default. Then core pockets serve to initiate pocket communities; each isolated core pocket or each set of overlapping core pockets is designated as a community core. Each community core is then expanded to include any overlapping auxiliary pockets. Each expanded set of core and auxiliary pockets is designated as a pocket community. This protocol does allow for pocket overlap between distinct communities; overlapping communities are not consolidated. To qualify as overlapping pockets—in both core pocket consolidation and auxiliary pocket expansion—a pair of pockets must satisfy two requirements: (1) share at least one pocket atom and (2) if the pockets point away from each other, the angle between their directional pocket vectors cannot be greater than 90°. The second requirement strengthens the prediction of pocket community cotargetability; this is included to avoid grouping together pockets that do share atoms but face opposite directions. A pocket's directional vector, a novel AlphaSpace descriptor, is defined from the centroid of its pocket atoms to the centroid of its alpha-cluster. The community score, which is the sum of all pocket scores (core and auxiliary) within a community, can be used to help detect potentially druggable protein surface regions.

RESULTS

We first utilized the well-studied Mdm2/p53 PPI as a test case to retrospectively demonstrate how AlphaSpace fragment-centric topographical mapping (FCTM) can be employed to facilitate rational PPI inhibitor design. The Mdm2/p53 PPI offers an attractive model because of the availability of high-resolution structures for the native PPI as well as for Mdm2 bound to a biomimetic inhibitor, bound to a small molecule fragment-based inhibitor, and in the apo protein state. We evaluate the ability of AlphaSpace to identify hot spot-associated pockets at the four interfaces and to detect and match important auxiliary interaction regions. We then evaluate the application of AlphaSpace to a larger data set of 12 PPI, 12 iPPI, and 9 apo structures from the 2P2I database; this data set was curated to represent systems successfully targeted by and crystallized with small molecule PPI inhibitors.[68,69] We confirm that high-ranking fragment-centric pockets are generally enriched at PPI and iPPI interfaces, which we leverage using *Pocket communities* to identify the iPPI interfaces from surface structures alone. We demonstrate that *Pocket matching* between sets of PPI/iPPI/apo protein structures allows us to identify and track similar pockets at a fragment-centric resolution to

DOI: 10.1021/acs.jcim.5b00103
J. Chem. Inf. Model. 2015, 55, 1585−1599

rank	color	score	% occupied	alpha-space	% nonpolar
1	green	241	72%	250	97%
2	yellow	189	94%	241	78%
3	pink	154	33%	187	83%
4	teal	39	51%	70	56%
5	orange	39	71%	44	89%
6	blue	14	88%	55	25%
7	purple	12	100%	13	94%

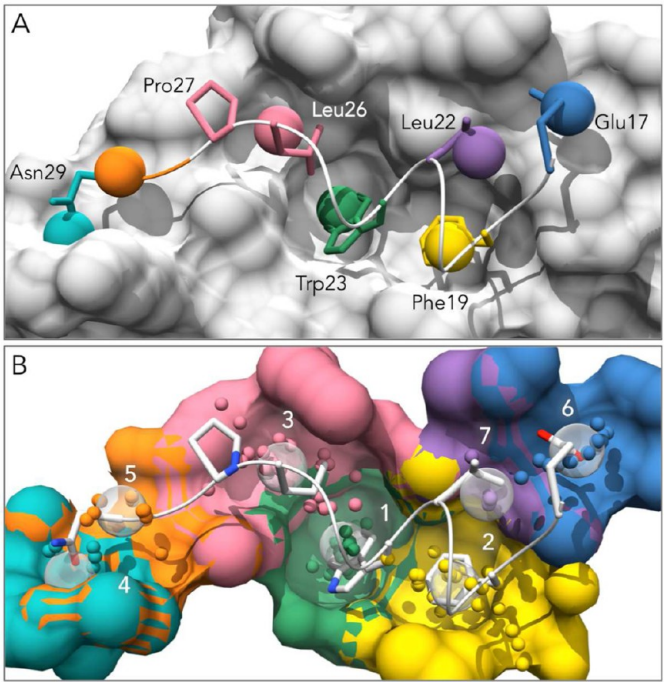

Figure 4. *Pocket Ranking.* Alpha-space-based pocket features are presented for the seven contact pockets at the Mdm2/p53 PPI interface. (A, B) Different visual representations of the FCTM result for Mdm2/p53. (A) Interface pockets are represented by the centroid of each alpha-cluster. The side chains from p53 are displayed and labeled whenever they make contact with one of the interface pockets, and pocket-fragment interactions are color-coordinated. The natural modularity of the surface is exhibited in the overlap between the centroids and the side chains. (B) Each pocket is represented as a surface, alpha sphere centers are shown as small spheres colored by pocket, and the alpha-cluster centroids are depicted as large transparent spheres. Pockets are numbered by rank, as in the table.

measure pocket flexibility and to characterize the structural integrity of the surface at functional interfaces.

Mdm2/p53: Pocket Ranking. Mdm2/p53 is an important PPI and oncogene drug target, with several small molecule inhibitors currently in clinical trials.[80] Its PPI interface is formed between a 13-residue helical section from the N-terminal transactivation domain of p53 and a well-defined binding groove in the surface of Mdm2. This interaction is known to be anchored by three primary hot spot residues from p53—Phe19, Trp23, Leu26—and a secondary hydrophobic interaction with Leu22.[81]

As shown in Figure 4, AlphaSpace FCTM detects a total of seven contact pockets in the surface of Mdm2 at the Mdm2/p53 interface. Aside from pocket 3, which is occupied by the side-chains of Leu26 and Pro27, and pocket 5, which interacts with the backbone of p53, the other five pockets each clearly contact a single side chain from p53. There is a distinct spatial overlap between the alpha-cluster centroids and the pocket-bound peptide fragments. This indicates an innate structural modularity in the protein surface that reflects the corresponding side chain interactions. It should be noted that such a complete and fragment-centric characterization of the Mdm2/p53 interface was not achieved using fpocket with the default parameters. As shown in Figure S1B, the corresponding fpocket analysis detects a single pocket in the surface of Mdm2 at the Mdm2/p53 interface, spanning the Trp23, Leu26, and Pro27 interactions, and does not account for the important Mdm2 interactions with Phe19 or Leu22 of p53.

For the seven AlphaSpace pockets, the calculated pocket features—pocket score, percent occupied, total alpha-space, and percent nonpolar—are presented in Figure 4. The pockets are ranked and numbered by pocket score. We find that pocket 1 (score = 241; 72% occupied) and pocket 2 (score = 189; 94% occupied) engage the two essential hot spot residues Trp23 and Phe19 of p53, respectively. The less occupied pocket 3 (score = 154; 33% occupied) engages the third but less dominant hot spot residue Leu26. These results are consistent with the experimental alanine-scanning data for p53,[81] as shown in Table S2, in which mutation of either Phe19 or Trp23 reduces the Mdm2/p53 binding affinity below the detectable limit and Leu26/Ala mutagenesis results in a significant reduction of binding affinity by more than 50 fold. Meanwhile, the Leu22 of p53, whose alanine mutagenesis results in a 10-fold decrease in Mdm2/p53 binding affinity, interacts with the lowest ranked pocket 7 (score = 12; 100% occupied). The targeting of a low-scoring pocket by an important residue underscores that a truly complete pocket analysis depends on the surface mapping of both binding partners. Either surface may simultaneously function as both pocket and ligand, even for a helix-in-groove PPI such as Mdm2/p53. When we, inversely, map the surface of the p53 helix, we find Leu22 is involved in the formation of the most significant p53 pocket (score = 37, 75% occupied), which, in the complex, binds Val69 from Mdm2 (Figure S6). Thus, in targeting a small auxiliary pocket, Leu22 also completes the formation of an important interaction region on p53, enriching the quality of the total PPI interaction.

The values for several other pocket-centric and ligand-centric descriptors are listed in Table S3, including atom counts, polar atom counts, presence of charged species, and the residue IDs of the contact fragments. Additionally, results for the FCTM of a second well-studied system, the Bcl-xL/Bak PPI interface, are presented in the Supporting Information. Table S5 reports the experimental alanine scanning data for the Bak helical interaction domain. Figure S16 illustrates the FCTM of the

DOI: 10.1021/acs.jcim.5b00103
J. Chem. Inf. Model. 2015, 55, 1585−1599

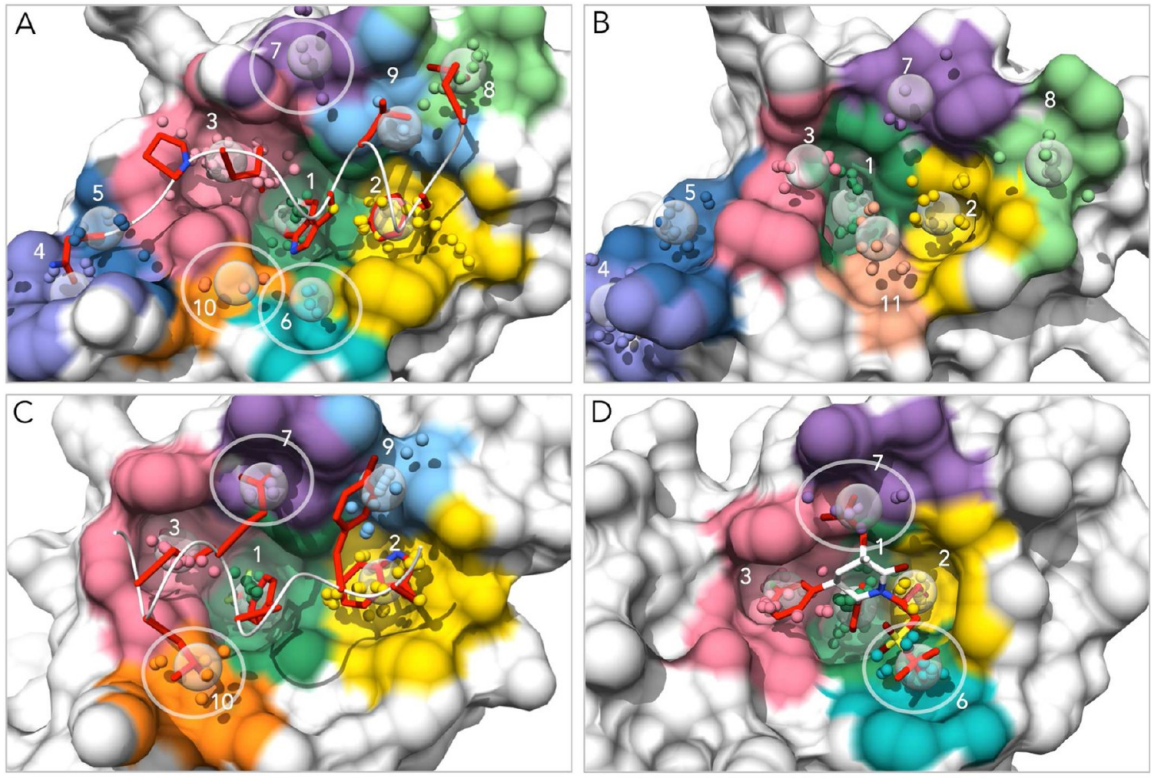

		(A) Mdm2/p53		(B) Mdm2(apo)			(C) Mdm2/D-peptide			(D) Mdm2/small mol		
index	color	score	%occ	sim	score	%occ	sim	score	%occ	sim	score	%occ
1	green	241	72%	0.39	108	n/a	0.77	261	81%	0.73	299	95%
2	yellow	189	94%	0.41	86	n/a	0.54	114	96%	0.44	78	100%
3	pink	154	33%	0.39	25	n/a	0.39	114	81%	0.40	130	98%
4	peri	39	51%	0.27	37	n/a						
5	blue	39	71%	0.38	55	n/a						
6	teal	22	0%							0.49	36	100%
7	purple	17	0%	0.29	3	n/a	0.46	10	100%	0.48	15	34%
8	ltgreen	14	88%	0.25	3	n/a						
9	ltblue	12	100%				0.37	24	66%			
10	orange	5	0%				0.65	15	53%			
11	peach			n/a	46	n/a						

Figure 5. *Pocket matching.* (A) Mdm2/p53, (B) Mdm2 apo, (C) Mdm2/^{D}PMI-δ ($_{D}$-peptide inhibitor), and (D) Mdm2/piperidinone sulfone derivative (small molecule inhibitor). Topographical maps of the interfaces are illustrated; matching pockets are color coordinated and numbered. Circled in (A) are three unoccupied pockets identified near the PPI interface. Pockets circled in (C) and (D) match with the unoccupied pockets from (A) but are now targeted by inhibitor fragments. The table presents the matching results for all pockets, including similarity (calculated in reference to the matching Mdm2/p53 pocket), pocket score, and percent pocket occupation.

Bcl-xL surface at the PPI interface. Again, structural modularity can be observed in the overlap between the interacting side chains of Bak and the alpha-cluster centroids. The two highest scoring pockets correspond to the two primary Bak hot spots—Leu78 and Ile85—and the two moderately high scoring pockets correspond to two of the three secondary Bak hot spots—Val74 and Ile81. (The final secondary hot spot—Asp83—extends into the solution, away from the PPI interface.) The additional pocket-centric and ligand-centric features for Bcl-xL/Bak are presented in Table S6.

Mdm2/p53: Pocket Matching. The Mdm2/p53 interface has been effectively targeted using both fragment-based and biomimetic inhibitor design. The nutlins, a set of cis-imidazoline small molecules that mimic the four main interaction points, were the first inhibitors discovered to modulate Mdm2/p53.[63] Subsequent FBDD efforts led to the discovery of the current ultrahigh affinity inhibitors that optimize these primary interactions and introduce additional, novel interaction points.[27,82−84]

We have selected two iPPI structures of Mdm2 in complex with ultrahigh-affinity inhibitors emerging from each of these design strategies: a small fragment-based molecule (a piperidinone sulfone derivative) with IC_{50} 0.10 nM[27] (PDB: 4oas) and a D-peptide antagonist (^{D}PMI-δ) with K_d 0.22 nM[84] (PDB: 3tpx). Figure 5 displays the mapping of each of these interfaces, along with those of the native Mdm2/p53 PPI[85] (PDB: 1ycr) and the apo state of Mdm2[86] (PDB: 1z1m). This Mdm2/p53 map has been expanded to include unoccupied pockets near the interface in addition to p53 contact pockets. The same interface atom list from Mdm2/p53 was used to select for pockets in the apo structure. For the two iPPIs, all ligand contact pockets are shown. *Pocket matching* is performed

DOI: 10.1021/acs.jcim.5b00103
J. Chem. Inf. Model. 2015, 55, 1585−1599

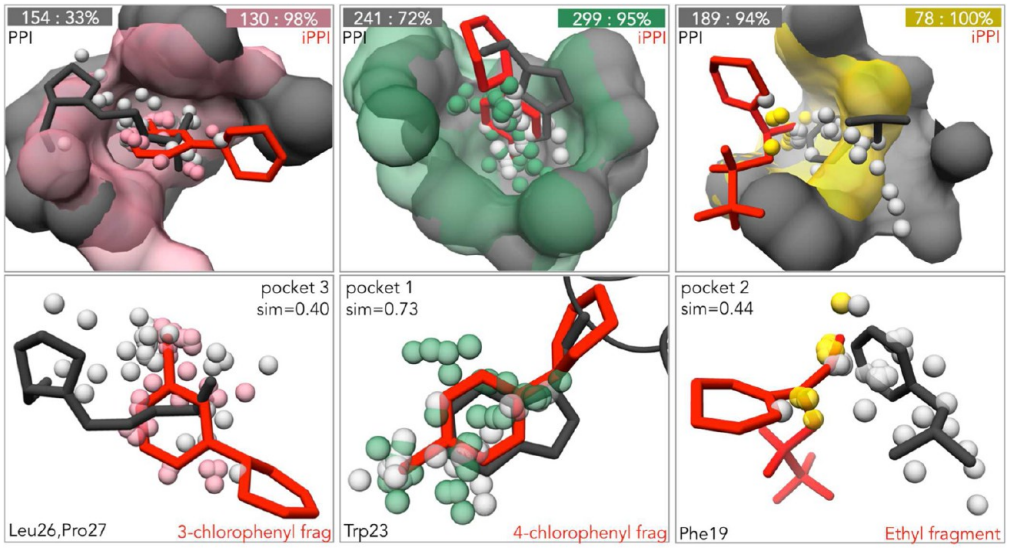

Figure 6. *Pocket-fragment complementarity.* Pocket alignments between Mdm2/p53 (PPI) and Mdm2/small molecule inhibitor (iPPI) for pockets 1 (center), 2 (right), and 3 (left). PPI: pockets (gray), alpha-centers (light gray), and bound residues (dark gray). iPPI: pockets (pink, green, yellow), alpha spheres (pink, green, yellow), and bound fragments (red). In the top panels, we specify the score and the percent occupation for each pocket in the color-coded top bars. In the bottom panels, we specify the calculated similarity for each pocket pair, and we specify the bound residues from the native PPI and the bound chemical fragments from the iPPI.

on the four Mdm2 structures collectively, and the result is presented in Figure 5.

In the development of these picomolar inhibitors, mirror image phage display with chemical ligation[83,87] and fragment-based screening methods[82] led to the identification of three auxiliary interaction sites in the vicinity of the Mdm2/p53 interface but not utilized in the native Mdm2/p53 PPI. These are an acetate fragment binding region adjacent to the Leu22 interaction site (targeted by both inhibitors), a hydrophobic patch on the opposite side of the helix between the Trp23 and Leu26 binding pockets (targeted by ^{D}PMI-δ), and the "glycine shelf", which is adjacent to the Phe19 binding pocket (targeted by the small molecule inhibitor). FCTM of these interfaces not only identifies each of these interaction regions as distinct pockets in the corresponding iPPIs, but identifies all three interaction regions as unoccupied pockets in the native Mdm2/p53 interface: pocket 7, pocket 10, and pocket 6, respectively (Figure 5A).

The targeting of pocket 7, despite its low pocket score, significantly enhances the affinity of both inhibitors by introducing favorable electrostatic interactions between the acetate fragment and Lys94, His96, and, for ^{D}PMI-δ, His73. The affinity enhancement due to this fragment is roughly 20-fold for the small molecule inhibitor[82] and, for ^{D}PMI-α, a predecessor to ^{D}PMI-δ, the alanine mutation of this acetate side chain reduces affinity by about 10-fold.[83] For ^{D}PMI-α, the alanine mutation of the Leu10, which targets pocket 10, reduces affinity by 4.5-fold. Pocket 10 has a particularly low pocket score, but, as with Leu22 of p53 discussed above, the targeting of this pocket forms a reciprocal pocket in the surface of ^{D}PMI-δ (score = 40) that is filled by Leu54 from Mdm2 (Figure S7). The specific affinity enhancement due to the targeting of pocket 6 by the *tert*-butyl fragment of the small molecule inhibitor is difficult to assess independently since this fragment and the ethyl fragment occupying pocket 2 were modified in tandem,[27] but the initial targeting of this pocket in the development of its predecessor, AM-8553, enhanced affinity about 20-fold.[82] Overall, this indicates that the targeting of small, auxiliary pockets, detectable using AlphaSpace, can facilitate the productive design of competitive PPI inhibitors.

Mdm2/p53: Pocket-Fragment Complementarity. The top three pockets from the Mdm2/p53 interface are associated with the primary hot spot residues from p53 and can be matched with three similar pockets from the iPPI interface between Mdm2 and the ultrahigh-affinity small molecule inhibitor (Figure 6). Using *Pocket-fragment complementarity*, we measure improvements for all three pockets between the native PPI and the optimized iPPI. For pocket 1 and pocket 3, by individually aligning the matching pockets using the positions of shared pocket atoms, we can visualize the spatial relationship between the unoccupied subspace detected in the native PPI and the corresponding occupied space in the iPPI. From the alignment of pocket 1, we observe the phenyl ring from the 4-chlorophenyl inhibitor fragment is aligned with the six-member ring of Trp23. The chloro fragment on the inhibitor extends directly into the unoccupied space identified near Trp23, and the pocket-fragment complementarity improves from 72% occupied in the PPI to 95% occupied in the iPPI. For pocket 3, occupation is only 33% in the PPI; neither of the interacting residues (Leu26, Pro27) is optimally positioned to extend into the core of the pocket, leaving considerable unoccupied interaction space. Alternatively, the 3-chlorophenyl fragment from the inhibitor approaches the pocket from a different angle, and the halogen extends directly into the space unoccupied in the PPI, boosting pocket occupation to 98%. Regarding pocket 2, the conservation of high pocket-fragment complementarity between the PPI and the iPPI (94% and 100% respectively) is a good example of functional pocket flexibility. This pocket, expanded in the PPI to accommodate the bulky side chain of Phe19, collapses significantly in the iPPI in response to the smaller ethyl fragment, retaining complementarity with the ligand. As highlighted in Figure 7, the structural mechanism for this pocket flexibility is driven primarily by loop dynamics.

Mdm2/p53: Comparison to FTMap. FTMap[56,57] is a computational solvent mapping software used to identify high

DOI: 10.1021/acs.jcim.5b00103
J. Chem. Inf. Model. 2015, 55, 1585−1599

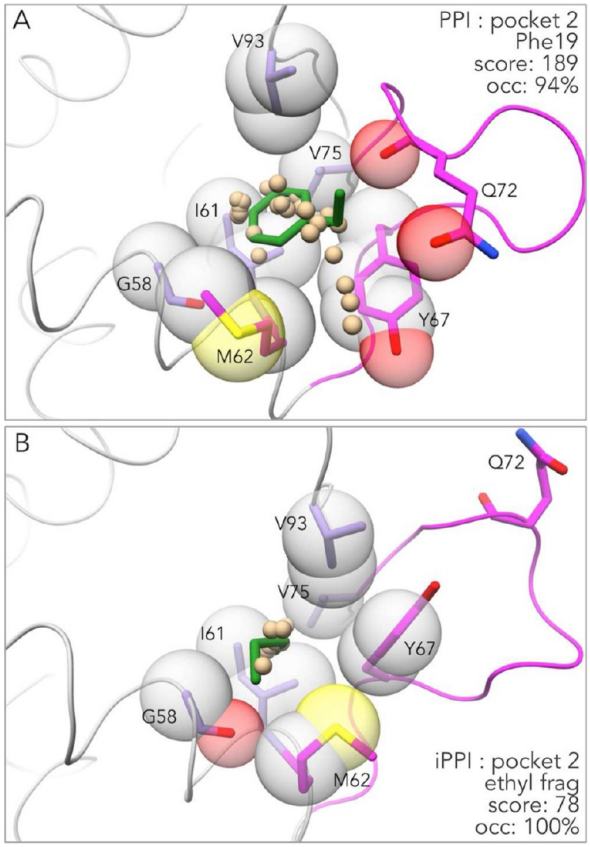

Figure 7. Residue-centric visualization of flexible pocket 2 at the Mdm2/p53 PPI (A) and the Mdm2/small molecule inhibitor iPPI (B). Pocket defining residues are shown in stick representation, labeled, and colored light purple if structurally stable or magenta if structurally variant between pockets. Pocket defining atoms are shown as transparent VdW spheres colored by atom type. The peptide fragment (A) and inhibitor fragment (B) that bind to pocket 2 are shown in green, and the alpha-atom centers are represented as small tan spheres.

quality interaction space at the protein surface. By virtue of its fragment-docking algorithm, FTMap employs a naturally fragment-centric approach. We compare the topographical mapping results for the Mdm2 interfaces under study with the corresponding FTMap results (Figure S8). In general, the results from the two methods are remarkably consistent. The interaction regions detected by FTMap at the interfaces of Mdm2 overlap precisely with alpha-clusters detected by AlphaSpace, and aside from a few instances, the overlapping interaction regions are described at a similar resolution (i.e., one AlphaSpace alpha-cluster overlaps with one FTMap probe cluster). However, we observe that AlphaSpace provides more comprehensive coverage of the interaction interfaces. Several small auxiliary pockets, detected by AlphaSpace and directly targeted by the inhibitors we have discussed, go undetected in the FTMap results. Additionally, for the apo state of Mdm2, FTMap identifies only two of the seven pockets detected by AlphaSpace. These unidentified pockets generally exhibit lower fragment-targetability, but their detection is critical to achieve a comprehensive and continuous map of the interface. Overall, the clear agreement between methods in identifying and localizing high-quality interaction regions is very encouraging given the strength of the FTMap results published in the literature.[59,88]

2P2I Data Set: Pocket Ranking. In order to evaluate the performance of FCTM applied to a larger data set, we used AlphaSpace to map a total of 33 protein surfaces (12 PPIs, 12 iPPIs, and 9 apo structures) taken from the 2P2I database.[69] These PPIs exhibit a diverse set of interfacial structures including various α helix, β sheet, and loop motifs. If multiple iPPI complexes were available for the same protein, we selected the complex corresponding to the highest affinity inhibitor. (See Table S1 for the complete list of PDB IDs used in the analysis and the Supporting Information regarding the two systems omitted due to incompatibility.)

AlphaSpace maps provide comprehensive coverage of PPI/iPPI interfaces. On average, 89% and 95% of all interfacial surface area is characterized for PPIs and iPPIs, respectively, by the sets of fragment-centric contact pockets engaged in binding at the interfaces (Table S4). To confirm the enrichment of high-ranking pockets at the PPI/iPPI interfaces, we mapped the entire protein surface of each structure (for the 12 matching PPI/iPPI pairs) into fragment-centric interaction regions and then scored and ranked each pocket among all other pockets in that protein. We evaluated the rankings for the subset of pockets found at the PPI/iPPI interfaces. As shown in Figure 8A, "high-ranking" pockets (90th percentile and above) are

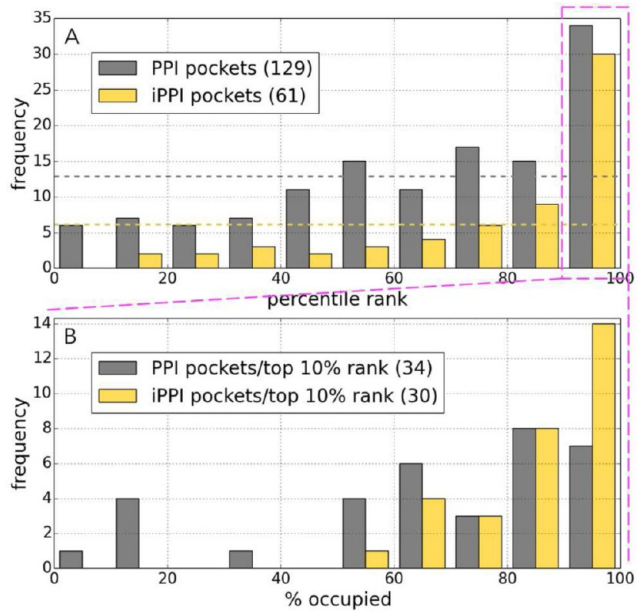

Figure 8. (A) Histograms illustrating the distributions for the percentile rankings of all interface pockets for 12 PPIs (gray) and 12 iPPIs (yellow); ranking is based on pocket scores. Dashed gray and yellow lines represent the statistically expected, uniform distributions for PPIs and iPPIs, respectively. High-ranking pockets are enriched for both sets. (B) Histograms illustrating the distributions for the percent occupations of all high-ranking (90th percentile or above) PPI (gray) and iPPI (yellow) interface pockets. Percent occupation is calculated as the portion of a pocket's alpha-space that is associated with alpha spheres in contact with peptide or inhibitor atoms.

sharply enriched at the interfaces of the PPIs and the iPPIs, appearing 2.6 and 4.9 times their expected values. The higher enrichment and lower pocket count at iPPI interfaces indicate that PPI inhibitors do target high-scoring AlphaSpace pockets.

2P2I Data Set: Pocket-Fragment Complementarity. We also evaluated the complementarity between high-ranking PPI/iPPI pockets and the peptide or inhibitor fragments they

DOI: 10.1021/acs.jcim.5b00103
J. Chem. Inf. Model. 2015, 55, 1585−1599

bind. Pocket-fragment complementarity is expressed as the percent occupation of a pocket, calculated as described in the Methods section. Figure 8B illustrates that, generally, high-ranking PPI and iPPI interface pockets bind to their respective fragments with moderate to high complementarity. However, there is a distinct shift for high-ranking iPPI pockets toward higher pocket occupation; 47% of high-ranking iPPI pockets are occupied above 90% compared to 20% of high-ranking PPI pockets. Better complementarity may contribute to the generally high ligand efficiency (LE) documented for successful iPPIs.[23] Furthermore, from an inhibitor design perspective, partially unoccupied PPI pockets represent opportunities to optimize affinity over the native interactions.

2P2I Data Set: Pocket Communities. To leverage the observed enrichment of high-scoring pockets at iPPIs, AlphaSpace uses *Pocket communities*, as described in the Methods section, to search the protein surface for overlapping clusters of high-scoring pockets. This method is intended to detect fragment-based drug-targetable surface regions from the surface structure alone. To validate the application, we evaluated the performance of *Pocket communities* to identify the known druggable surface regions from the 12 iPPIs in our 2P2I data set. In 8 out of 12 structures, the iPPI interface is identified as the #1 ranked pocket community; in 11 out of 12 structures, the iPPI interface is identified in the top 3 ranked pocket communities. In 9 out of the 11 identified iPPIs, the druggable interface is represented by a single pocket community; otherwise, two pocket communities represent the interface. Table 1 shows the high precision in our detection of the druggable interfaces. For 10 out of 11 predicted iPPI interfaces, the pocket communities account for 100% of the core and auxiliary pockets in contact with the ligand. And for the 11 identified iPPI interface, there are, on average, 2.1 unoccupied pockets included in the corresponding pocket communities. In practice, these unoccupied pockets may represent viable auxiliary pockets yet to be targeted. (See Figure 9 to visualize the druggable pocket communities identified for two example systems: TNFalpha and Bcl-xL.)

Table 1. *Pocket Communities* Identified at iPPI Interfaces Are Listed by Their Rank with the Number of Pockets (core + auxiliary) per Community[a]

	pocket communities at iPPI interfaces		pocket community coverage of iPPI interface pockets		
system	rank	#pock	#pock cover	#pock miss	#pock out
Bcl-2	1,2	5,3	5	0	1
Bcl-xL	1	11	8	0	3
HPV-E2	1	8	4	0	4
Il-2	2	2	2	1	0
Integr.	1	6	3	0	3
Mdm2	1	5	5	0	0
Mdm4	1	5	4	0	1
Menin	3,5	7,5	3	0	8
TNFa	2	5	3	0	2
Xdm2	1	3	3	0	0
Xiap	1	4	2	0	1
ZipA	-	-	0	1	-

[a]To evaluate the overlap between the pocket communities and the set of core and auxiliary contact pockets from each iPPI interface, we list the number of interface pockets covered by the communities, the number of interface pockets missed by the communities, and the number of community pockets that fall outside the direct iPPI interfaces.

We also test the performance of *Pocket communities* to detect drug-targetable communities in the corresponding apo structures near the known iPPI interfaces. For 5 out of 9 apo structures, the druggable interface can still be identified as the #1 ranked pocket community, and 1 more interface is identified by the #2 ranked pocket community. For the remaining three apo structures—Il-2, Bcl-xL, and ZipA—no pocket communities are identified at the known iPPI interfaces. To clarify, an interface will not register as a pocket community unless at least one core pocket can be detected. However, for the three apo interfaces that do not register as pocket communities, we do observe several fragment-centric pockets scoring very close to the core pocket score cutoff, indicating that the method is sensitive to their latent druggability. We believe that the inability to detect high targetability at these particular interfaces is probably an accurate result for the apo states, especially given a previous report that several apo conformations of targeted iPPI interfaces require the rotation of interfacial side chains to improve their targetability.[57]

2P2I Data Set: Pocket Matching. Next, we evaluated the performance of *Pocket matching* as a model to track pockets at a fragment-centric resolution between PPI, iPPI, and apo structures for the nine systems with available structures for all three states. This allows us to assess the degree of structural conservation or flexibility at the protein surface between the apo structure and the complex structures. For the apo structures, we only include pockets in contact with the inhibitor compound from the corresponding iPPI after superimposing the iPPI structure onto the apo structure. The motivation here is to explore the ability of AlphaSpace to identify and assess, specifically, pockets in each apo structure that are near the verified druggable interaction regions from the iPPIs. (See Figure S9 for a visual representation of the pocket matching results for all nine systems.) Figure 10 presents, as an example, the pocket matching results for Menin, which exhibits well-conserved pockets across all three surface states. Figure S10 illustrates, for TNFalpha, how the surface structure can change at the fragment-centric resolution from the apo interface to the iPPI interface.

The results from Table 2 indicate that there are, on average, 4.3 fragment-centric pockets detected near the druggable surface region for each apo structure in the data set, and most of these pockets, 79%, can be matched to binding pockets identified in the iPPI structures. Comparing the apo vs iPPI pocket scores for the set of 31 pockets that match between iPPI and apo structures reveals that, while 58% of the fragment-centric pockets do exhibit reduced scores in the apo structures, which reflects the general expectation that pockets are attenuated in apo surfaces, 23% of the apo pockets exhibit higher scores than the matching pockets at the iPPI interfaces, and 19% exhibit similar pocket scores between the two states.

There are, on average, 11 fragment-centric pockets identified at each PPI interface (this drops to 8.3 if TNFalpha is omitted which has the largest PPI interface with 33 fragment-centric pockets), and roughly half of this pocket count, 5.1 pockets on average, is identified at iPPI interfaces. Seventy-five percent of all iPPI pockets can be matched to pockets identified in the native PPIs. Interestingly, among these 34 pockets that match between the PPIs and iPPIs, 41% exhibit higher scores in the iPPI, 41% exhibit lower scores in the iPPI, and 18% exhibit similar pocket scores. This result indicates that many pockets

DOI: 10.1021/acs.jcim.5b00103
J. Chem. Inf. Model. 2015, 55, 1585−1599

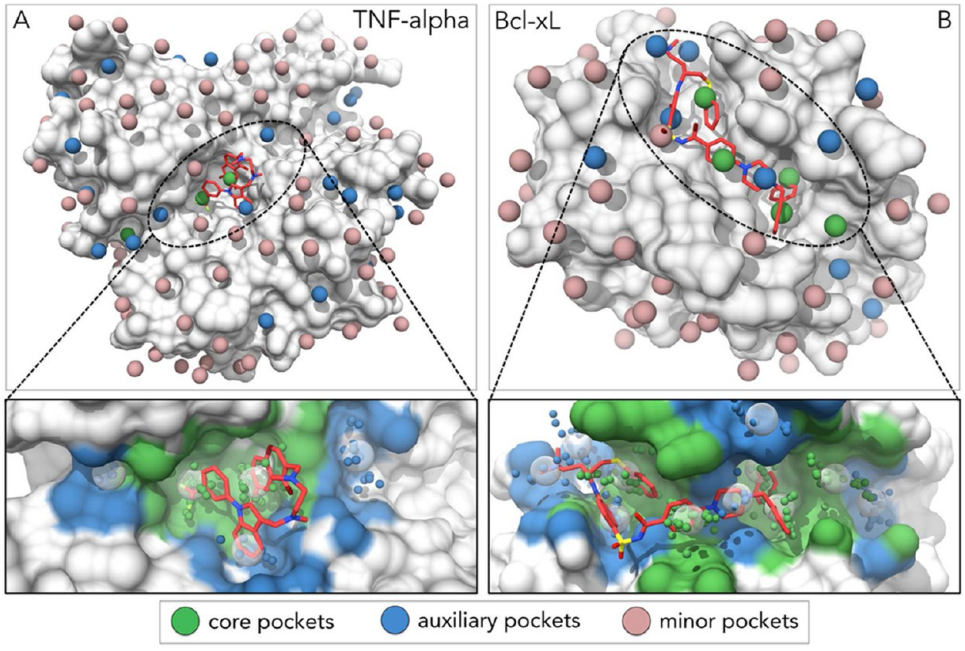

Figure 9. *Pocket communities* are identified as high-scoring clusters of core and auxiliary pockets and represent potentially druggable surface regions. In the top panels, we visualize all fragment-centric pockets across the surfaces of two example proteins: TNF-alpha (A) and Bcl-xL (B). Each pockets is represented by a single sphere positioned at the centroid of its alpha-cluster; the spheres are colored by pocket classification: core pockets (green), auxiliary pockets (blue), and minor pockets (rosy brown). The respective fragment-based inhibitors are displayed in red. In the bottom panels, we zoom in to highlight the specific pocket communities identified at the known iPPI interfaces. For each core and auxiliary pocket in each community, we now show the detailed alpha-cluster as small spheres (colored by pocket classification), and the alpha-cluster centroids are now shown as transparent larger spheres. Pocket atoms in the surface of the proteins are colored by pocket classification. The TNF-alpha pocket community (left) contains two core pockets, three auxiliary pockets, and community score = 368. The Bcl-xL pocket community (right) contains 5 core pockets, 6 auxiliary pockets, and community score = 1208.

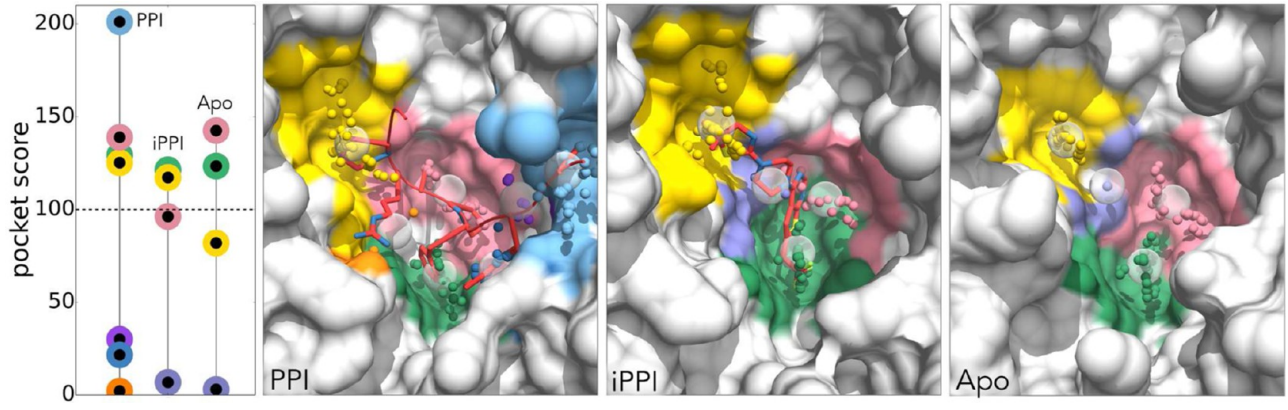

Figure 10. *Pocket matching* example between the PPI, iPPI, and apo protein surfaces of Menin. (Left) Each fragment-centric pocket at the respective interface is represented by a colored ring along the pocket score axis: PPI (left), iPPI (center), and apo (right). Matching pockets are designated by matching ring color. In the surface structures to the right, alpha-clusters and pocket atoms are colored to match their respective ring colors. Alpha-cluster centroids are shown as transparent spheres. Binding partners are shown in red. The green, yellow, and pink pockets are well conserved across all three surface states.

are conserved between these structures but still the interfaces tend to adapt differently to the different binding partners. Furthermore, 25% of all iPPI pockets are distinct from pockets detected in the PPIs, which also highlights the flexibility at functional interfaces and the ability of AlphaSpace to detect when an inhibitor has targeted a novel pocket. On average, there are 2.6 pockets per system that match between all three protein structure states.

2P2I Data Set: Ligand−Alpha-Cluster Volume/Shape Correlation. In order to highlight the capacity for alpha-clusters to serve as mock molecular binders, we evaluate the volumetric correlation and shape similarity between the bound PPI inhibitors and the corresponding sets of contact alpha-clusters. For the correlation between the total contact alpha-cluster volume and the total ligand volume, we calculate r = 0.77. This demonstrates a general volumetric correlation, but to evaluate the mock ligand feature more precisely, we can omit from the calculated volumes the specific alpha-atoms representing unoccupied interaction space as well as parts of the inhibitor molecule not in direct contact with the surface (i.e., outside 4.5 Å from the protein surface). For this corrected correlation between the occupied alpha-atom volume and the

DOI: 10.1021/acs.jcim.5b00103
J. Chem. Inf. Model. 2015, 55, 1585−1599

Table 2. *Pocket Matching* Results for the 2P2I Dataset[a]

	# interface pockets			# pockets matched between			
system	PPI	iPPI	Apo	PPI-iPPI	iPPI-apo	PPI-apo	all 3
Bcl-2	13	6	5	5	4	3	3
Bcl-xL	13	10	7	6	5	3	3
Il-2	9	6	4	3	4	2	2
Integr	6	3	5	2	3	3	2
Mdm2	7	5	5	3	3	3	2
Menin	7	4	4	3	4	3	3
TNFa	33	3	2	3	2	2	2
Xiap	4	4	4	4	3	3	3
ZipA	7	5	3	5	3	3	3
mean	11	5.1	4.3	3.8	3.4	2.8	2.6

[a](Left) Total number of fragment-centric pockets identified at each PPI, iPPI, and apo interface. (Right) Matching pocket counts between each possible combination of the three surface states: PPI and iPPI, iPPI and apo, PPI and apo, or matching across all three states.

surface-contact ligand volume, we calculate r = 0.92. Furthermore, as shown in Figure 11, the linear fit for these corrected volumes is quite similar to the line $y = x$. This result demonstrates that alpha-clusters roughly approximate the actual size of corresponding molecular ligands. In Figure 11, we show the overlapping alpha-cluster and inhibitor structures for three example systems—Bcl-xL, Il-2, and Xiap—in order to illustrate the global shape similarity between the inhibitors and each set of occupied alpha-atoms.

DISCUSSION

AlphaSpace represents a departure from existing geometry-based pocket detection in two central aspects. The first is our emphasis on providing a comprehensive map of interaction space across the molecular interface of interest. The map is not limited to hot spots but extends to cover all concave interaction regions engaged in binding and can be systematically expanded further to reveal unoccupied, targetable pockets near the interface. The conventional cavity-centric approach is to screen out what is appraised as insignificant interaction space and deliver only a small set of the highest-ranking pockets. However, as shown for the high-affinity Mdm2/p53 iPPIs, small auxiliary pockets can provide guidance for the extension of fragment-based inhibitors and can provide opportunities to enhance ligand affinity and selectivity. Demonstrated for the protein targets in the 2P2I database, AlphaSpace can effectively match and track pockets between the apo, PPI, and iPPI states, detecting pocket conservation as well as pocket modulation between conformations. Pocket matching provides a model to study the dynamic integrity of functional interfaces and to characterize interface flexibility at a fragment-centric resolution.

The second major divergence of AlphaSpace is our development of a fragment-centric strategy compared to the long-standing cavity-centric approach. We have found that PPI interfaces are more accurately comprised of arrays of shallow pockets, which exhibit more subtle spatial separation than classical binding sites, but can still contribute to overall binding affinity and are likely to dictate the details of interaction selectivity. The experimental strategies used to target these surfaces are evolving from traditional compound screening approaches to fragment-based screening approaches. This shift has facilitated the successful development of a number of high affinity compounds with unique molecular scaffolds.[23] The fragment-centric design of AlphaSpace is a direct response to this methodological shift. Our strategy is to subdivide broad

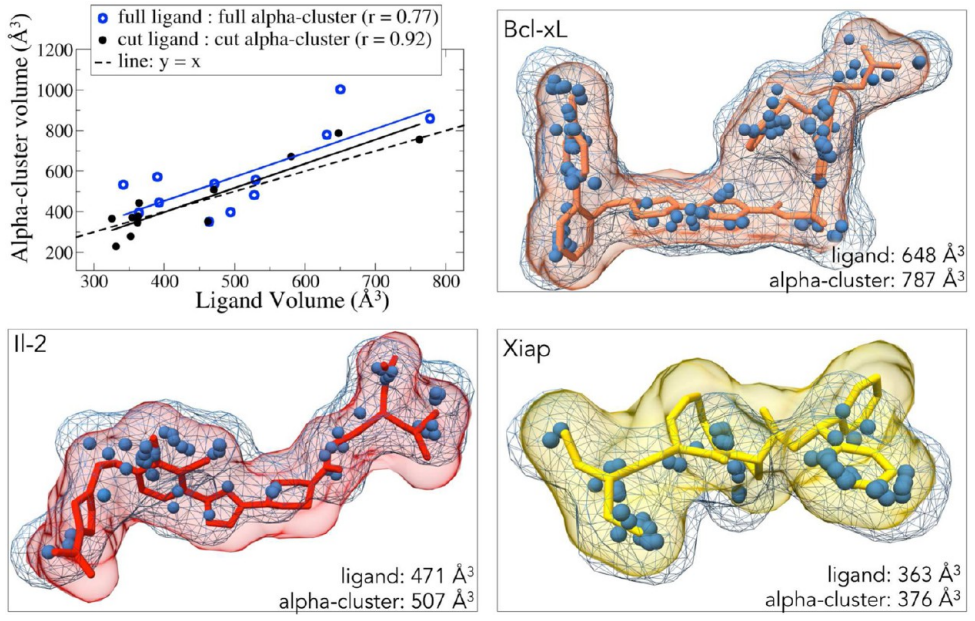

Figure 11. (Top left) The correlation between ligand volume and contact alpha-cluster volume is plotted and evaluated for 12 iPPIs from the 2P2I database. In blue, we plot the full ligand volume against the volume of the full alpha-cluster after merging the alpha-atoms of all ligand-contact pockets (r = 0.77). In black, we plot the volume for a reduced set of ligand atoms, excluding ligand atoms not in contact with the protein surface, against the reduced alpha-cluster, excluding alpha-atoms not in contact with the ligand (r = 0.92). We use three example systems to illustrate the shape similarity between the ligands that bind to each of these systems and the corresponding cluster of contact alpha-atoms from the mapping of each iPPI interface: Bcl-xL (orange), Il-2 (red), and Xiap (yellow). Alpha-atom centers are shown as small blue spheres, and the shape of each contact alpha-cluster is shown in blue wire representation. The ligands are shown simultaneously in stick representation and as transparent molecular surfaces. The volumes listed are for the reduced ligand and the reduced alpha-cluster.

DOI: 10.1021/acs.jcim.5b00103
J. Chem. Inf. Model. 2015, 55, 1585−1599

PPI interfaces into localized fragment-centric interaction regions, reflecting the types of pockets targeted with FBDD. In addition, at this fragment-centric resolution, AlphaSpace evaluates pocket-fragment complementarity to pinpoint unoccupied interaction space for fragment optimization.

Accounting for the complete determinants of PPI affinity is a complex challenge; however, the primary roles of the hydrophobic effect and of VdW interactions have been established and robustly reiterated within the literature.[75,89−92] The AlphaSpace pocket score is not intended to be a definitive, nor absolute, PPI/iPPI scoring function. At the least, a more accurate interaction analysis will require the integration of more explicit electrostatic and desolvation terms. Rather, our pocket score was developed to be a practical metric reflecting two key structural features related to the hydrophobic effect—nonpolar surface area and pocket curvature—to discern the approximate, relative targetabilities of fragment-centric interaction regions. Importantly, the scoring function is calculated from the surface structure alone, allowing for the screening of any protein surface to search for highly targetable pocket communities as potential starting points for fragment-based inhibitor development.

CONCLUSION

The therapeutic modulation of protein−protein interactions represents an important and rapidly expanding field of scientific research. AlphaSpace fragment-centric topographical mapping (FCTM) is a new alpha sphere-based pocket detection tool designed to provide a high-resolution visual and quantitative characterization of all interaction space at a PPI interface. We have illustrated how several attractive features of AlphaSpace can facilitate the rational design and optimization of fragment-based or biomimetic PPI inhibitors. AlphaSpace is implemented in Python, and a copy can be obtained free of charge for academic use from http://www.nyu.edu/projects/yzhang/AlphaSpace. We hope that AlphaSpace FCTM will become a useful tool for the community to assist in the discovery of novel and potent PPI inhibitors.

ASSOCIATED CONTENT

Supporting Information

The Supporting Information is available free of charge on the ACS Publications website at DOI: 10.1021/acs.jcim.5b00103.

Figures, tables, implementation and parametrization details, and results for the FCTM of a second system, the Bcl-xL/Bak PPI interface. (PDF)

AUTHOR INFORMATION

Corresponding Author

*E-mail: yingkai.zhang@nyu.edu.

Notes

The authors declare no competing financial interest.

ACKNOWLEDGMENTS

We acknowledge support from NIH (R01-GM079223 to Zhang, R01GM073943 to Arora). We thank NYU-ITS and NYUAD for providing computational resources. Molecular images were generated with the UCSF Chimera package.[93]

REFERENCES

(1) Arkin, M. Protein-Protein Interactions and Cancer: Small Molecules Going in for the Kill. *Curr. Opin. Chem. Biol.* **2005**, *9*, 317−324.
(2) Nero, T. L.; Morton, C. J.; Holien, J. K.; Wielens, J.; Parker, M. W. Oncogenic Protein Interfaces: Small Molecules, Big Challenges. *Nat. Rev. Cancer* **2014**, *14*, 248−262.
(3) Lao, B. B.; Grishagin, I.; Mesallati, H.; Brewer, T. F.; Olenyuk, B. Z.; Arora, P. S. In Vivo Modulation of Hypoxia-Inducible Signaling by Topographical Helix Mimetics. *Proc. Natl. Acad. Sci. U. S. A.* **2014**, *111*, 7531−7536.
(4) Sundaram, J. R.; Poore, C. P.; Sulaimee, N. H. B.; Pareek, T.; Asad, A. B. M. A.; Rajkumar, R.; Cheong, W. F.; Wenk, M. R.; Dawe, G. S.; Chuang, K.-H.; Pant, H. C.; Kesavapany, S. Specific Inhibition of p25/Cdk5 Activity by the Cdk5 Inhibitory Peptide Reduces Neurodegeneration in Vivo. *J. Neurosci.* **2013**, *33*, 334−343.
(5) Blazer, L. L.; Neubig, R. R. Small Molecule Protein-Protein Interaction Inhibitors as CNS Therapeutic Agents: Current Progress and Future Hurdles. *Neuropsychopharmacology* **2009**, *34*, 126−141.
(6) Goldberg, B.; Bona, C. Dimeric MHC-Peptides Inserted into an Immunoglobulin Scaffold as New Immunotherapeutic Agents. *J. Cell. Mol. Med.* **2011**, *15*, 1822−1832.
(7) Braisted, A. C.; Oslob, J. D.; Delano, W. L.; Hyde, J.; McDowell, R. S.; Waal, N.; Yu, C.; Arkin, M. R.; Raimundo, B. C. Discovery of a Potent Small Molecule IL-2 Inhibitor through Fragment Assembly. *J. Am. Chem. Soc.* **2003**, *125*, 3714−3715.
(8) He, M. M.; Smith, A. S.; Oslob, J. D.; Flanagan, W. M.; Braisted, A. C.; Whitty, A.; Cancilla, M. T.; Wang, J.; Lugovskoy, A. A.; Yoburn, J. C.; Fung, A. D.; Farrington, G.; Eldredge, J. K.; Day, E. S.; Cruz, L. A.; Cachero, T. G.; Miller, S. K.; Friedman, J. E.; Choong, I. C.; Cunningham, B. C. Small-Molecule Inhibition of TNF-Alpha. *Science* **2005**, *310*, 1022−1025.
(9) Hayouka, Z.; Rosenbluh, J.; Levin, A.; Loya, S.; Lebendiker, M.; Veprintsev, D.; Kotler, M.; Hizi, A.; Loyter, A.; Friedler, A. Inhibiting HIV-1 Integrase by Shifting Its Oligomerization Equilibrium. *Proc. Natl. Acad. Sci. U. S. A.* **2007**, *104*, 8316−8321.
(10) Goudreau, N.; Cameron, D. R.; Déziel, R.; Haché, B.; Jakalian, A.; Malenfant, E.; Naud, J.; Ogilvie, W. W.; O'meara, J.; White, P. W.; Yoakim, C. Optimization and Determination of the Absolute Configuration of a Series of Potent Inhibitors of Human Papillomavirus Type-11 E1-E2 Protein-Protein Interaction: A Combined Medicinal Chemistry, NMR and Computational Chemistry Approach. *Bioorg. Med. Chem.* **2007**, *15*, 2690−2700.
(11) Tsao, D. H. H.; Sutherland, A. G.; Jennings, L. D.; Li, Y.; Rush, T. S.; Alvarez, J. C.; Ding, W.; Dushin, E. G.; Dushin, R. G.; Haney, S. A.; Kenny, C. H.; Malakian, A. K.; Nilakantan, R.; Mosyak, L. Discovery of Novel Inhibitors of the ZipA/FtsZ Complex by NMR Fragment Screening Coupled with Structure-Based Design. *Bioorg. Med. Chem.* **2006**, *14*, 7953−7961.
(12) Cochran, A. Antagonists of Protein-Protein Interactions. *Chem. Biol.* **2000**, *7*, R85−R94.
(13) Spencer, R. W. High-Throughput Screening of Historic Collections: Observations on File Size, Biological Targets, and File Diversity. *Biotechnol. Bioeng.* **1998**, *61*, 61−67.
(14) Whitty, A.; Kumaravel, G. Between a Rock and a Hard Place? *Nat. Chem. Biol.* **2006**, *2*, 112−118.
(15) Tan, D. S. Diversity-Oriented Synthesis: Exploring the Intersections between Chemistry and Biology. *Nat. Chem. Biol.* **2005**, *1*, 74−84.
(16) Arkin, M. R.; Tang, Y.; Wells, J. A. Small-Molecule Inhibitors of Protein-Protein Interactions: Progressing toward the Reality. *Chem. Biol.* **2014**, *21*, 1102−1114.
(17) Azzarito, V.; Long, K.; Murphy, N. S.; Wilson, A. J. Inhibition of A-Helix-Mediated Protein-Protein Interactions Using Designed Molecules. *Nat. Chem.* **2013**, *5*, 161−173.
(18) Milroy, L.-G.; Grossmann, T. N.; Hennig, S.; Brunsveld, L.; Ottmann, C. Modulators of Protein-Protein Interactions. *Chem. Rev.* **2014**, *114*, 4695−4748.

(19) Murray, C. W.; Rees, D. C. The Rise of Fragment-Based Drug Discovery. *Nat. Chem.* **2009**, *1*, 187−192.
(20) Congreve, M.; Chessari, G.; Tisi, D.; Woodhead, A. J. Recent Developments in Fragment-Based Drug Discovery. *J. Med. Chem.* **2008**, *51*, 3661−3680.
(21) Shuker, S. B.; Hajduk, P. J.; Meadows, R. P.; Fesik, S. W. Discovering High-Affinity Ligands for Proteins: SAR by NMR. *Science* **1996**, *274*, 1531−1534.
(22) Raimundo, B. C.; Oslob, J. D.; Braisted, A. C.; Hyde, J.; McDowell, R. S.; Randal, M.; Waal, N. D.; Wilkinson, J.; Yu, C. H.; Arkin, M. R. Integrating Fragment Assembly and Biophysical Methods in the Chemical Advancement of Small-Molecule Antagonists of IL-2: An Approach for Inhibiting Protein-Protein Interactions. *J. Med. Chem.* **2004**, *47*, 3111−3130.
(23) Wells, J. A.; McClendon, C. L. Reaching for High-Hanging Fruit in Drug Discovery at Protein-Protein Interfaces. *Nature* **2007**, *450*, 1001−1009.
(24) Mullard, A. Protein−protein Interaction Inhibitors Get into the Groove. *Nat. Rev. Drug Discovery* **2012**, *11*, 173−175.
(25) Fuller, J. C.; Burgoyne, N. J.; Jackson, R. M. Predicting Druggable Binding Sites at the Protein-Protein Interface. *Drug Discovery Today* **2009**, *14*, 155−161.
(26) Aguilar, A.; Zhou, H.; Chen, J.; Liu, L.; Bai, L.; McEachern, D.; Yang, C.-Y.; Meagher, J.; Stuckey, J.; Wang, S. A Potent and Highly Efficacious Bcl-2/Bcl-xL Inhibitor. *J. Med. Chem.* **2013**, *56*, 3048−3067.
(27) Sun, D.; Li, Z.; Rew, Y.; Gribble, M.; Bartberger, M. D.; Beck, H. P.; Canon, J.; Chen, A.; Chen, X.; Chow, D.; Deignan, J.; Duquette, J.; Eksterowicz, J.; Fisher, B.; Fox, B. M.; Fu, J.; Gonzalez, A. Z.; Gonzalez-Lopez De Turiso, F.; Houze, J. B.; Huang, X.; Jiang, M.; Jin, L.; Kayser, F.; Liu, J. J.; Lo, M.-C.; Long, A. M.; Lucas, B.; McGee, L. R.; McIntosh, J.; Mihalic, J.; Oliner, J. D.; Osgood, T.; Peterson, M. L.; Roveto, P.; Saiki, A. Y.; Shaffer, P.; Toteva, M.; Wang, Y.; Wang, Y. C.; Wortman, S.; Yakowec, P.; Yan, X.; Ye, Q.; Yu, D.; Yu, M.; Zhao, X.; Zhou, J.; Zhu, J.; Olson, S. H.; Medina, J. C. Discovery of AMG 232, a Potent, Selective, and Orally Bioavailable MDM2-p53 Inhibitor in Clinical Development. *J. Med. Chem.* **2014**, *57*, 1454−1472.
(28) Bogan, A. A.; Thorn, K. S. Anatomy of Hot Spots in Protein Interfaces. *J. Mol. Biol.* **1998**, *280*, 1−9.
(29) Kortemme, T.; Kim, D. E.; Baker, D. Computational Alanine Scanning of Protein-Protein Interfaces. *Sci. Signaling* **2004**, *2004*, pl2.
(30) Koes, D. R.; Camacho, C. J. PocketQuery: Protein-Protein Interaction Inhibitor Starting Points from Protein-Protein Interaction Structure. *Nucleic Acids Res.* **2012**, *40*, W387−W392.
(31) Moreira, I. S.; Fernandes, P. A.; Ramos, M. J. Hot Spots−a Review of the Protein-Protein Interface Determinant Amino-Acid Residues. *Proteins: Struct., Funct., Genet.* **2007**, *68*, 803−812.
(32) Raj, M.; Bullock, B. N.; Arora, P. S. Plucking the High Hanging Fruit: A Systematic Approach for Targeting Protein-Protein Interactions. *Bioorg. Med. Chem.* **2013**, *21*, 4051−4057.
(33) Watkins, A. M.; Arora, P. S. Structure-Based Inhibition of Protein-Protein Interactions. *Eur. J. Med. Chem.* **2015**, *94*, 480−488.
(34) Binkowski, T. A.; Naghibzadeh, S.; Liang, J. CASTp: Computed Atlas of Surface Topography of Proteins. *Nucleic Acids Res.* **2003**, *31*, 3352−3355.
(35) Peters, K. P.; Fauck, J.; Frömmel, C. The Automatic Search for Ligand Binding Sites in Proteins of Known Three-Dimensional Structure Using Only Geometric Criteria. *J. Mol. Biol.* **1996**, *256*, 201−213.
(36) Le Guilloux, V.; Schmidtke, P.; Tuffery, P. Fpocket: An Open Source Platform for Ligand Pocket Detection. *BMC Bioinf.* **2009**, *10*, 168.
(37) Laskowski, R. A. SURFNET: A Program for Visualizing Molecular Surfaces, Cavities, and Intermolecular Interactions. *J. Mol. Graphics* **1995**, *13*, 323−330.
(38) Brady, G. P., Jr.; Stouten, P. F. Fast Prediction and Visualization of Protein Binding Pockets with PASS. *J. Comput.-Aided Mol. Des.* **2000**, *14*, 383−401.
(39) Yu, J.; Zhou, Y.; Tanaka, I.; Yao, M. Roll: A New Algorithm for the Detection of Protein Pockets and Cavities with a Rolling Probe Sphere. *Bioinformatics* **2010**, *26*, 46−52.
(40) Hernandez, M.; Ghersi, D.; Sanchez, R. SITEHOUND-Web: A Server for Ligand Binding Site Identification in Protein Structures. *Nucleic Acids Res.* **2009**, *37*, W413−W416.
(41) Laurie, A. T. R.; Jackson, R. M. Q-SiteFinder: An Energy-Based Method for the Prediction of Protein-Ligand Binding Sites. *Bioinformatics* **2005**, *21*, 1908−1916.
(42) Halgren, T. A. Identifying and Characterizing Binding Sites and Assessing Druggability. *J. Chem. Inf. Model.* **2009**, *49*, 377−389.
(43) An, J.; Totrov, M.; Abagyan, R. Pocketome via Comprehensive Identification and Classification of Ligand Binding Envelopes. *Mol. Cell. Proteomics* **2005**, *4*, 752−761.
(44) Levitt, D. G.; Banaszak, L. J. POCKET: A Computer Graphics Method for Identifying and Displaying Protein Cavities and Their Surrounding Amino Acids. *J. Mol. Graphics* **1992**, *10*, 229−234.
(45) Hendlich, M.; Rippmann, F.; Barnickel, G. LIGSITE: Automatic and Efficient Detection of Potential Small Molecule-Binding Sites in Proteins. *J. Mol. Graphics Modell.* **1997**, *15*, 359−363.
(46) Huang, B.; Schroeder, M. LIGSITEcsc: Predicting Ligand Binding Sites Using the Connolly Surface and Degree of Conservation. *BMC Struct. Biol.* **2006**, *6*, 19.
(47) Weisel, M.; Proschak, E.; Schneider, G. PocketPicker: Analysis of Ligand Binding-Sites with Shape Descriptors. *Chem. Cent. J.* **2007**, *1*, 7.
(48) Marks, D. S.; Colwell, L. J.; Sheridan, R.; Hopf, T. A.; Pagnani, A.; Zecchina, R.; Sander, C. Protein 3D Structure Computed from Evolutionary Sequence Variation. *PLoS One* **2011**, *6*, e28766.
(49) Durrant, J. D.; De Oliveira, C. A. F.; McCammon, J. A. POVME: An Algorithm for Measuring Binding-Pocket Volumes. *J. Mol. Graphics Modell.* **2011**, *29*, 773−776.
(50) Ngan, C.-H.; Hall, D. R.; Zerbe, B.; Grove, L. E.; Kozakov, D.; Vajda, S. FTSite: High Accuracy Detection of Ligand Binding Sites on Unbound Protein Structures. *Bioinformatics* **2012**, *28*, 286−287.
(51) Li, H.; Kasam, V.; Tautermann, C. S.; Seeliger, D.; Vaidehi, N. Computational Method to Identify Druggable Binding Sites That Target Protein-Protein Interactions. *J. Chem. Inf. Model.* **2014**, *54*, 1391−1400.
(52) Chang, D. T.-H.; Oyang, Y.-J.; Lin, J.-H. MEDock: A Web Server for Efficient Prediction of Ligand Binding Sites Based on a Novel Optimization Algorithm. *Nucleic Acids Res.* **2005**, *33*, W233−W238.
(53) Huang, N.; Jacobson, M. P. Binding-Site Assessment by Virtual Fragment Screening. *PLoS One* **2010**, *5*, e10109.
(54) Schmidtke, P.; Souaille, C.; Estienne, F.; Baurin, N.; Kroemer, R. T. Large-Scale Comparison of Four Binding Site Detection Algorithms. *J. Chem. Inf. Model.* **2010**, *50*, 2191−2200.
(55) Laurie, A. T. R.; Jackson, R. M. Methods for the Prediction of Protein-Ligand Binding Sites for Structure-Based Drug Design and Virtual Ligand Screening. *Curr. Protein Pept. Sci.* **2006**, *7*, 395−406.
(56) Brenke, R.; Kozakov, D.; Chuang, G.-Y.; Beglov, D.; Hall, D.; Landon, M. R.; Mattos, C.; Vajda, S. Fragment-Based Identification of Druggable "Hot Spots" of Proteins Using Fourier Domain Correlation Techniques. *Bioinformatics* **2009**, *25*, 621−627.
(57) Kozakov, D.; Hall, D. R.; Chuang, G.-Y.; Cencic, R.; Brenke, R.; Grove, L. E.; Beglov, D.; Pelletier, J.; Whitty, A.; Vajda, S. Structural Conservation of Druggable Hot Spots in Protein-Protein Interfaces. *Proc. Natl. Acad. Sci. U. S. A.* **2011**, *108*, 13528−13533.
(58) Zerbe, B. S.; Hall, D. R.; Vajda, S.; Whitty, A.; Kozakov, D. Relationship between Hot Spot Residues and Ligand Binding Hot Spots in Protein-Protein Interfaces. *J. Chem. Inf. Model.* **2012**, *52*, 2236−2244.
(59) Hall, D. R.; Ngan, C. H.; Zerbe, B. S.; Kozakov, D.; Vajda, S. Hot Spot Analysis for Driving the Development of Hits into Leads in Fragment-Based Drug Discovery. *J. Chem. Inf. Model.* **2012**, *52*, 199−209.

DOI: 10.1021/acs.jcim.5b00103
J. Chem. Inf. Model. 2015, 55, 1585−1599

(60) Volkamer, A.; Griewel, A.; Grombacher, T.; Rarey, M. Analyzing the Topology of Active Sites: On the Prediction of Pockets and Subpockets. *J. Chem. Inf. Model.* **2010**, *50*, 2041−2052.
(61) Volkamer, A.; Kuhn, D.; Grombacher, T.; Rippmann, F.; Rarey, M. Combining Global and Local Measures for Structure-Based Druggability Predictions. *J. Chem. Inf. Model.* **2012**, *52*, 360−372.
(62) Molecular Operating Environment (MOE), 2013.08; Chemical Computing Group, Inc.: Montreal, QC, Canada, 2014.
(63) Vassilev, L. T.; Vu, B. T.; Graves, B.; Carvajal, D.; Podlaski, F.; Filipovic, Z.; Kong, N.; Kammlott, U.; Lukacs, C.; Klein, C.; Fotouhi, N.; Liu, E. A. In Vivo Activation of the p53 Pathway by Small-Molecule Antagonists of MDM2. *Science* **2004**, *303*, 844−848.
(64) Zhao, Y.; Aguilar, A.; Bernard, D.; Wang, S. Small-Molecule Inhibitors of the MDM2-p53 Protein-Protein Interaction (MDM2 Inhibitors) in Clinical Trials for Cancer Treatment. *J. Med. Chem.* **2015**, *58*, 1038−1052.
(65) Sattler, M. Structure of Bcl-xL-Bak Peptide Complex: Recognition Between Regulators of Apoptosis. *Science (Washington, DC, U. S.)* **1997**, *275*, 983−986.
(66) Degterev, A.; Lugovskoy, A.; Cardone, M.; Mulley, B.; Wagner, G.; Mitchison, T.; Yuan, J. *Nat. Cell Biol.* **2001**, *3*, 173−182.
(67) Liang, J.; Edelsbrunner, H.; Woodward, C. Anatomy of Protein Pockets and Cavities: Measurement of Binding Site Geometry and Implications for Ligand Design. *Protein Sci.* **1998**, *7*, 1884−1897.
(68) Bourgeas, R.; Basse, M.-J.; Morelli, X.; Roche, P. Atomic Analysis of Protein-Protein Interfaces with Known Inhibitors: The 2P2I Database. *PLoS One* **2010**, *5*, e9598.
(69) Basse, M. J.; Betzi, S.; Bourgeas, R.; Bouzidi, S.; Chetrit, B.; Hamon, V.; Morelli, X.; Roche, P. 2P2Idb: A Structural Database Dedicated to Orthosteric Modulation of Protein-Protein Interactions. *Nucleic Acids Res.* **2013**, *41*, D824−D827.
(70) Poupon, A. Voronoi and Voronoi-Related Tessellations in Studies of Protein Structure and Interaction. *Curr. Opin. Struct. Biol.* **2004**, *14*, 233−241.
(71) Richards, F. M. The Interpretation of Protein Structures: Total Volume, Group Volume Distributions and Packing Density. *J. Mol. Biol.* **1974**, *82*, 1−14.
(72) Barber, C. B.; Dobkin, D. P.; Huhdanpaa, H. The Quickhull Algorithm for Convex Hulls. *ACM Trans. Math. Softw.* **1996**, *22*, 469−483.
(73) Jones, E.; Oliphant, T.; Peterson, P. SciPy: Open Source Scientific Tools for Python.
(74) Hubbard, S. J.; Thornton, J. M. *NACCESS, Computer Program, Department of Biochemistry and Molecular Biology*; University College: London, 1993.
(75) Cheng, A. C.; Coleman, R. G.; Smyth, K. T.; Cao, Q.; Soulard, P.; Caffrey, D. R.; Salzberg, A. C.; Huang, E. S. Structure-Based Maximal Affinity Model Predicts Small-Molecule Druggability. *Nat. Biotechnol.* **2007**, *25*, 71−75.
(76) Eyrisch, S.; Helms, V. Transient Pockets on Protein Surfaces Involved in Protein-Protein Interaction. *J. Med. Chem.* **2007**, *50*, 3457−3464.
(77) Rajamani, D.; Thiel, S.; Vajda, S.; Camacho, C. J. Anchor Residues in Protein-Protein Interactions. *Proc. Natl. Acad. Sci. U. S. A.* **2004**, *101*, 11287−11292.
(78) Meireles, L. M. C.; Dömling, A. S.; Camacho, C. J. ANCHOR: A Web Server and Database for Analysis of Protein-Protein Interaction Binding Pockets for Drug Discovery. *Nucleic Acids Res.* **2010**, *38*, W407−W411.
(79) Kozakov, D.; Hall, D. R.; Jehle, S.; Luo, L.; Ochiana, S. O.; Jones, E. V.; Pollastri, M.; Allen, K. N.; Whitty, A.; Vajda, S. Ligand Deconstruction: Why Some Fragment Binding Positions Are Conserved and Others Are Not. *Proc. Natl. Acad. Sci. U. S. A.* **2015**, *112*, E2585−E2594.
(80) Khoo, K. H.; Hoe, K. K.; Verma, C. S.; Lane, D. P. Drugging the p53 Pathway: Understanding the Route to Clinical Efficacy. *Nat. Rev. Drug Discovery* **2014**, *13*, 217−236.
(81) Li, C.; Pazgier, M.; Li, C.; Yuan, W.; Liu, M.; Wei, G.; Lu, W.-Y.; Lu, W. Systematic Mutational Analysis of Peptide Inhibition of the p53-MDM2/MDMX Interactions. *J. Mol. Biol.* **2010**, *398*, 200−213.
(82) Rew, Y.; Sun, D.; Gonzalez-Lopez De Turiso, F.; Bartberger, M. D.; Beck, H. P.; Canon, J.; Chen, A.; Chow, D.; Deignan, J.; Fox, B. M.; Gustin, D.; Huang, X.; Jiang, M.; Jiao, X.; Jin, L.; Kayser, F.; Kopecky, D. J.; Li, Y.; Lo, M.-C.; Long, A. M.; Michelsen, K.; Oliner, J. D.; Osgood, T.; Ragains, M.; Saiki, A. Y.; Schneider, S.; Toteva, M.; Yakowec, P.; Yan, X.; Ye, Q.; Yu, D.; Zhao, X.; Zhou, J.; Medina, J. C.; Olson, S. H. Structure-Based Design of Novel Inhibitors of the MDM2-p53 Interaction. *J. Med. Chem.* **2012**, *55*, 4936−4954.
(83) Liu, M.; Pazgier, M.; Li, C.; Yuan, W.; Li, C.; Lu, W. A Left-Handed Solution to Peptide Inhibition of the p53-MDM2 Interaction. *Angew. Chem., Int. Ed.* **2010**, *49*, 3649−3652.
(84) Zhan, C.; Zhao, L.; Wei, X.; Wu, X.; Chen, X.; Yuan, W.; Lu, W.-Y.; Pazgier, M.; Lu, W. An Ultrahigh Affinity D-Peptide Antagonist Of MDM2. *J. Med. Chem.* **2012**, *55*, 6237−6241.
(85) Kussie, P. H.; Gorina, S.; Marechal, V.; Elenbaas, B.; Moreau, J.; Levine, A. J.; Pavletich, N. P. Structure of the MDM2 Oncoprotein Bound to the p53 Tumor Suppressor Transactivation Domain. *Science* **1996**, *274*, 948−953.
(86) Uhrinova, S.; Uhrin, D.; Powers, H.; Watt, K.; Zheleva, D.; Fischer, P.; McInnes, C.; Barlow, P. N. Structure of Free MDM2 N-Terminal Domain Reveals Conformational Adjustments That Accompany p53-Binding. *J. Mol. Biol.* **2005**, *350*, 587−598.
(87) Dawson, P.; Muir, T.; Clark-Lewis, I.; Kent, S. Synthesis of Proteins by Native Chemical Ligation. *Science (Washington, DC, U. S.)* **1994**, *266*, 776−779.
(88) Zerbe, B. S.; Hall, D. R.; Vajda, S.; Whitty, A.; Kozakov, D. Relationship between Hot Spot Residues and Ligand Binding Hot Spots in Protein-Protein Interfaces. *J. Chem. Inf. Model.* **2012**, *52*, 2236−2244.
(89) Chothia, C.; Janin, J. Principles of Protein-Protein Recognition. *Nature* **1975**, *256*, 705−708.
(90) Nisius, B.; Sha, F.; Gohlke, H. Structure-Based Computational Analysis of Protein Binding Sites for Function and Druggability Prediction. *J. Biotechnol.* **2012**, *159*, 123−134.
(91) Kastritis, P. L.; Bonvin, A. M. J. J. On the Binding Affinity of Macromolecular Interactions: Daring to Ask Why Proteins Interact. *J. R. Soc., Interface* **2012**, *10*, 20120835.
(92) Cao, Y.; Li, L. Improved Protein-Ligand Binding Affinity Prediction by Using a Curvature-Dependent Surface-Area Model. *Bioinformatics* **2014**, *30*, 1674−1680.
(93) Pettersen, E. F.; Goddard, T. D.; Huang, C. C.; Couch, G. S.; Greenblatt, D. M.; Meng, E. C.; Ferrin, T. E. UCSF Chimera–a Visualization System for Exploratory Research and Analysis. *J. Comput. Chem.* **2004**, *25*, 1605−1612.

DOI: 10.1021/acs.jcim.5b00103
J. Chem. Inf. Model. 2015, 55, 1585−1599